Identification of Hemodynamically Optimal Coronary Stent Designs Based on Vessel Caliber

Timothy J. Gundert, Alison L. Marsden, Weiguang Yang, David S. Marks, and John F. LaDisa, Jr.*

***Abstract*—Coronary stent design influences local patterns of wall shear stress (WSS) that are associated with neointimal growth, restenosis, and the endothelialization of stent struts. The number of circumferentially repeating crowns N_C for a given stent design is often modified depending on the target vessel caliber, but the hemodynamic implications of altering N_C have not previously been studied. In this investigation, we analyzed the relationship between vessel diameter and the hemodynamically optimal N_C using a derivative-free optimization algorithm coupled with computational fluid dynamics. The algorithm computed the optimal vessel diameter, defined as minimizing the area of stent-induced low WSS, for various configurations (i.e., N_C) of a generic slotted-tube design and designs that resemble commercially available stents. Stents were modeled in idealized coronary arteries with a vessel diameter that was allowed to vary between 2 and 5 mm. The results indicate that the optimal vessel diameter increases for stent configurations with greater N_C, and the designs of current commercial stents incorporate a greater N_C than hemodynamically optimal stent designs. This finding suggests that reducing the N_C of current stents may improve the hemodynamic environment within stented arteries and reduce the likelihood of excessive neointimal growth and thrombus formation.**

***Index Terms*—Cardiovascular stent, computational fluid dynamics (CFD), coronary artery disease, optimization, restenosis, thrombus, wall shear stress (WSS).**

I. Introduction

TARGET vessel caliber is a known predictor of restenosis following stent implantation for the treatment of coronary artery disease [1], [2]. Rates of restenosis are significantly higher in patients with small diameter vessels since even a small amount of neointimal growth can severely restrict blood flow and require revascularization. Even when drug-eluting stents (DES) are used to inhibit neointimal growth, restenosis rates of 17% and 9.7% were reported in vessels with diameters $<$2.6 mm and $<$3 mm, respectively [3], [4]. Depending on the definition applied, treatment of small vessel lesions constitutes 35–67% of percutaneous interventions [5]. In contrast, large coronary vessels can sustain a greater amount of neointimal growth before requiring revascularization, and the use of DES over bare-metal stents in vessels $>$3.5 mm in diameter may not even be necessary [6].

Previous studies indicate stent-induced changes in local hemodynamics influence neointimal growth that leads to restenosis. Specifically, areas of low wall shear stress (WSS) and high oscillatory shear spatially correlate with regions of greatest intimal growth following stent implantation [7]–[9]. In addition to restenosis, the magnitude of WSS is known to affect the rate of endothelial cell migration atop stent struts [10]. Importantly, studies of DES in which re-endothelialization of stent struts is delayed suggest a lack of re-endothelialization is associated with an increased risk for thrombosis, which can lead to myocardial infarction [11]–[13]. Designing stents to reduce these hemodynamic disturbances would, therefore, decrease the likelihood of adverse long-term outcomes for lesion subsets that still have unfavorable outcomes.

Currently stent designs are often altered based on the vessel diameter in which the stent is deployed. While the underlying pattern of the stent design is not changed, the number of circumferentially repeating crowns or crests N_C is increased for vessels of a larger caliber and vice versa. For larger vessels, the increase in N_C provides more scaffolding and allows the stent to be expanded to a greater diameter. The hemodynamic implications of changing the stent configuration based on vessel diameter is unclear since previous studies of stent-induced blood flow alterations have largely used a nominal vessel diameter when modeling and analyzing stent design [14]–[16]. Computational fluid dynamics (CFD) studies of stent design indicate strut misalignment with the primary direction of flow results in localized areas of low WSS adjacent to struts [17], [18]. This suggests increasing N_C may be hemodynamically advantageous as it would reduce the degree of strut misalignment. In contrast, reducing N_C would increase the intrastrut area of the expanded stent, allowing for a greater area of flow reattachment and higher WSS between stent struts. We hypothesize there exists a hemodynamically optimal stent configuration in which the competing effects of strut misalignment and increasing intrastrut area are balanced. The optimal configuration is likely

Manuscript recieved December 17, 2011; revised March 23, 2012; accepted April 14, 2012. Date of publication April 25, 2012; date of current version June 20, 2012. This work was supported by a Translational Opportunity Grant of the Pilot and Collaborative Clinical and Translational Research Grants program from the Clinical and Translational Science Institute of Southeastern Wisconsin and computational support for this work was made possible by NSF under Grant CBET-0521602. The work of A. L. Marsden and W. Yang was supported by the Burroughs Wellcome Fund Career Award at the Scientific Interface. *Asterisk indicates corresponding author.*

T. J. Gundert is with the Department of Biomedical Engineering, Marquette University, Milwaukee, WI 53233 USA (e-mail: timothy.gundert@marquette.edu).

A. L. Marsden and W. Yang are with the Mechanical and Aerospace Engineering Department, University of California San Diego, La Jolla, CA 92093 USA (e-mail: amarsden@ucsd.edu; w1yang@ucsd.edu).

D. S. Marks is with the Division of Cardiovascular Medicine, Medical College of Wisconsin, Milwaukee, WI 53226 USA (e-mail: dmarks@mcw.edu).

*J. F. LaDisa, Jr., is with the Division of Pediatrics, Children's Hospital of Wisconsin, Division of Cardiovascular Medicine, Medical College of Wisconsin, and also with the Department of Biomedical Engineering, Marquette University, Milwaukee, WI 53233 USA (e-mail: john.ladisa@marquette.edu).

Color versions of one or more of the figures in this paper are available online at http://ieeexplore.ieee.org.

Digital Object Identifier 10.1109/TBME.2012.2196275

dependent on the vessel caliber and varies depending on the stent design.

In this investigation, we couple CFD with a derivative-free optimization framework to determine hemodynamically optimal stent configurations. To date, a majority of the studies that combine CFD with design optimization algorithms have only considered 2-D stent models or simple stent cells [19]–[21], such that the hemodynamic effects of vessel diameter and the N_C could not be studied. Pant *et al.* recently described a multiobjective stent optimization technique that uses 3-D models, but the study only considered 3-mm diameter vessels and a single stent design with a constant N_C [22]. The objective of this investigation was to analyze how vessel diameter affects the hemodynamically optimal N_C for several commercially available stent designs. We use our previously described optimization framework [23] to determine the optimal stent configuration, defined as the value of N_C that minimizes the area of low time-averaged WSS (TAWSS). Instead of maintaining a constant vessel diameter and computing the optimal stent configuration for numerous vessel diameters, in this investigation the optimization problem is framed to compute the optimal vessel diameter for a given N_C. Using this approach, the relationship between vessel diameter and the optimal stent design stent can be examined in more detail than using discrete vessel diameters.

II. Methods

A. Model Generation

The design of a generic slotted-tube stent (see Fig. 1: stent A) along with three designs that closely resemble commercially available stents (see Fig. 1: stents B–D) were investigated. Stents B and C were based on the BX Velocity (Cordis, Bridgewater, NJ) and Express^2 (Boston Scientific, Natick, MA) stents, respectively. Stent D was not based on any single stent design, but rather represented a simplified version of the Multi-Link family of stents (Abbott Vascular, Santa Clara, CA), which includes the Vision, Mini Vision, Ultra, and Zeta. The geometries of stents A, B, and D represent sequential ring stents with peak–peak (A and B) and peak–valley (D) connections [24]. Stent C is also a sequential ring stent, but the use of alternating "macro" and "micro" rings represents a hybrid of the peak–peak and peak–valley connection types.

The geometry of a single cell of each design is illustrated in Fig. 1 along with the dimensions relevant for approximating the expanded geometry of the stent, including the strut length l_s, arc length l_a, and connector length l_c. The dimensions of stents B, C, and D were based on the literature available on company websites and physical measurements. The circumferential distance between adjacent stent cells d and the intrastrut angle θ varied depending on the vessel diameter. The intrastrut angle was not used to define the cell geometry, but it was used extensively to quantify the results of the optimizations because it provides a design-independent measurement of the expanded stent geometry. The strut radial thickness and width for each design is given in Table I. All stents were modeled using the 18-mm version of the stent, with the exception of stent C, which was modeled as 16-mm since an 18-mm Express^2 stent is not available.

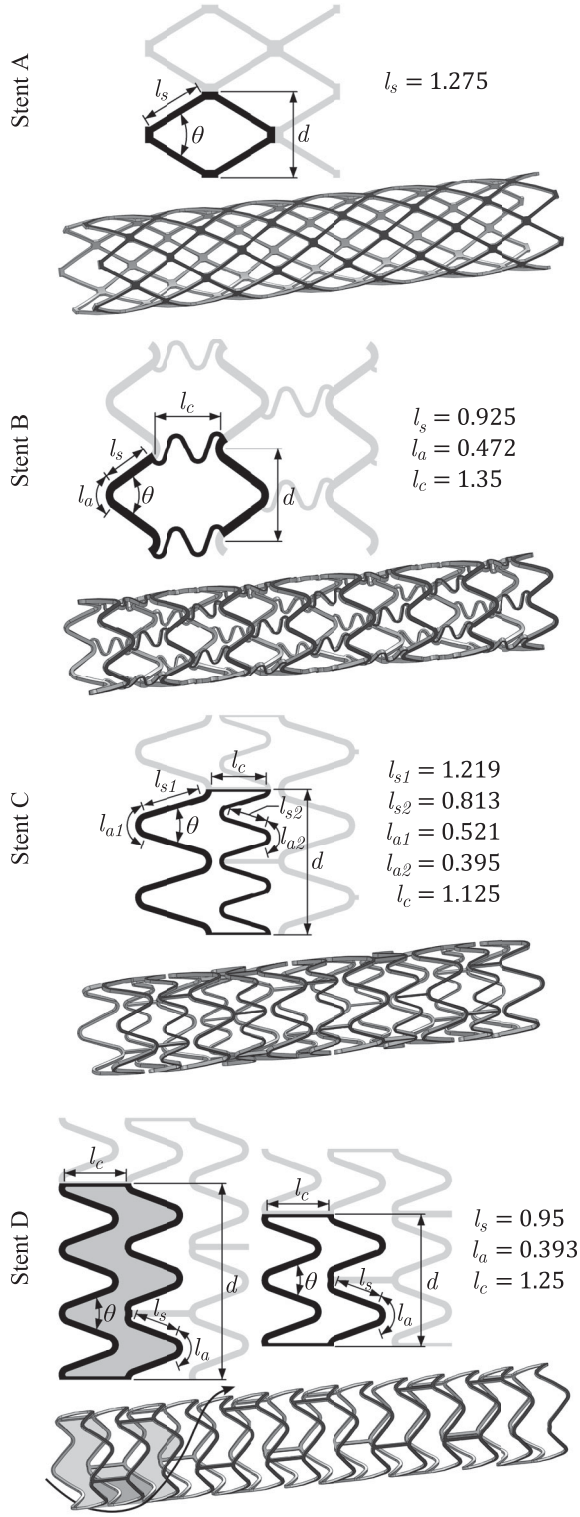

Fig. 1. Geometry of a single cell and related dimensions along with an expanded configuration of each stent design. All dimensions are given in millimeters. Each of the expanded stents shown has a diameter of 3.3 mm. Stents A, B, and C are shown in a six crown configuration, whereas stent D is shown in a five crown configuration that incorporates both the two and three crown cell geometries within each axially repeating segment of the stent. The arrangement of the two crown (white) and three crown (gray) cells is illustrated in two axially repeating segments of the expanded configurations of stent D. The axially repeating segments are offset from each other, which results in a slight twisting of the cell pattern along the length of stent D (denoted by the black arrow around the expanded configuration).

TABLE I
STRUT DIMENSIONS FOR EACH STENT DESIGN

Stent Design	Macro Struts		Micro (or link) Struts	
	Radial Thickness (μm)	Width (μm)	Radial Thickness (μm)	Width (μm)
A	100	100	-	-
B	140	143	140	60
C	132	91	132	61
D	81	100	-	-

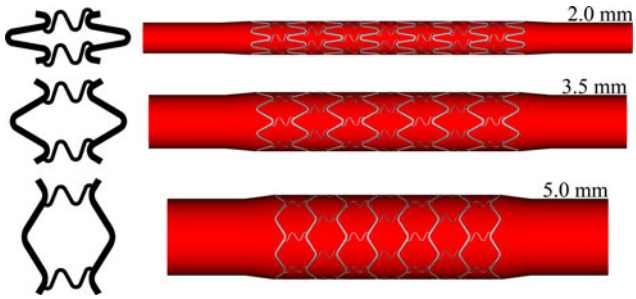

Fig. 2. Illustrations of the expanded geometry of single-stent cell (left) that were used to generate the three representative solids models of an idealized stented coronary (right). The vessel diameter depicted above each model corresponds to stent diameters of 2.2, 3.85, and 5.5 mm. The six crown configuration of stent B is depicted in each model.

In the case of stents A, B, and C, the number of circumferential repeating cells was simply varied to generate models with different values of N_C. It should be noted that N_C refers to the number of circumferentially repeating crowns, not the number of repeating cells. For example, the configuration of stent C shown in Fig. 1 has three circumferentially repeating cells, but each cell has two crowns resulting in $N_C = 6$. Because the commercial versions of stent D contain both two and three crown cell geometries, some permutations of stent D incorporated both cell geometries into an axial segment of the stent. Designs of stent D are denoted by both the number of crowns and the cells included in an axial segment in order to distinguish between the various permutations. For example, the five crown configuration of stent D in Fig. 1 is referred to as the 5-2:3 configuration because it includes both the two and three crown cell geometries. Similarly, the 6-2:2:2 and 6-3:3 both refer to six crown configurations constructed with only two crown and three crown cell geometries, respectively.

During the optimization of a single stent design, the stent configuration (i.e., N_C) was kept constant and the expanded geometry of the stent was modeled for the vessel diameters chosen by the optimization routine. For each model, the value of d was computed based on vessel diameter and N_C. The strut (l_s) and arc (l_a) lengths were kept constant to approximate the mechanical behavior of stent when it is expanded to various diameters. It was assumed the flexible link of stent B maintained its shape across all diameters. All stent models were generated using SolidWorks (Natick, MA).

Solid models of each vessel were constructed after the corresponding stent model was generated such that the expanded portion of the vessel could be modeled to the exact length of the expanded stent. In this manner, the effects of stent foreshortening would also be incorporated into the model (see Fig. 2). Vessels were modeled with a stent-to-artery ratio of 1.1:1 [25]. The vessel model proximal and distal to stented region consisted of a 5.0-mm unstented section of vessel connected to the stented region by a 2.0-mm tapered section [15]. Boolean subtraction was performed to remove the stent geometry from the vessel model resulting in a solid model of the flow domain.

B. Computational Fluid Dynamics

Stented vessels were discretized into unstructured tetrahedral finite-element meshes using a commercially available mesh generation program (MeshSim, Simmetrix, Clifton Park, NY). Anisotropic meshes were created for each stented artery model to best resolve the near-wall hemodynamics without incurring the high-computation cost associated with dense isotropic meshes. A relatively coarse mesh was prescribed to the unstented portion of the model while denser meshes were prescribed at the vessels walls within the stented portions of the vessel. The greatest mesh density was prescribed to the vessel wall in the middle segments of each stent because this is the only portion of the model quantified by the optimization algorithm (see Fig. 3).

It was not feasible to verify that the CFD results of each stented vessel model were independent of the mesh density because only one mesh was created for each model. The process of creating multiple meshes with increasing mesh densities to ensure mesh-independence would have drastically increased the computational expense of the optimization routine. Instead, we ensured the CFD results were independent of the mesh density by investigating the influence of meshing parameters on the solution (i.e., the optimal vessel diameter) of optimization algorithm for stent design B with $N_C = 5$. Briefly, an initial optimization was performed using mesh generation parameters that resulted in roughly 3–4 million element meshes for each model. A second optimization was then performed using parameters that created 6–8 million element meshes. The optimization converged to a vessel diameter of 2.625 mm, when high-density meshes were used compared to 2.656 mm for the low-density meshes. The greatest difference in cost was $<0.25\%$ between models with an equal vessel diameter, but different mesh density. Since doubling the mesh size only resulted in small variations in the computed cost and the optimal vessel diameter, the optimization results were assumed to be independent of the computational mesh, and the meshing parameters used to generate 3–4 million element meshes were used throughout the entire investigation.

Time-dependent CFD simulations were performed using an in-house stabilized finite-element solver with embedded commercial linear solver LESLIB (Altair Engineering, Troy, MI) to solve the time-dependent Navier–Stokes equations. A coronary waveform obtained from a canine left anterior descending artery was imposed at the model inlet using a fully

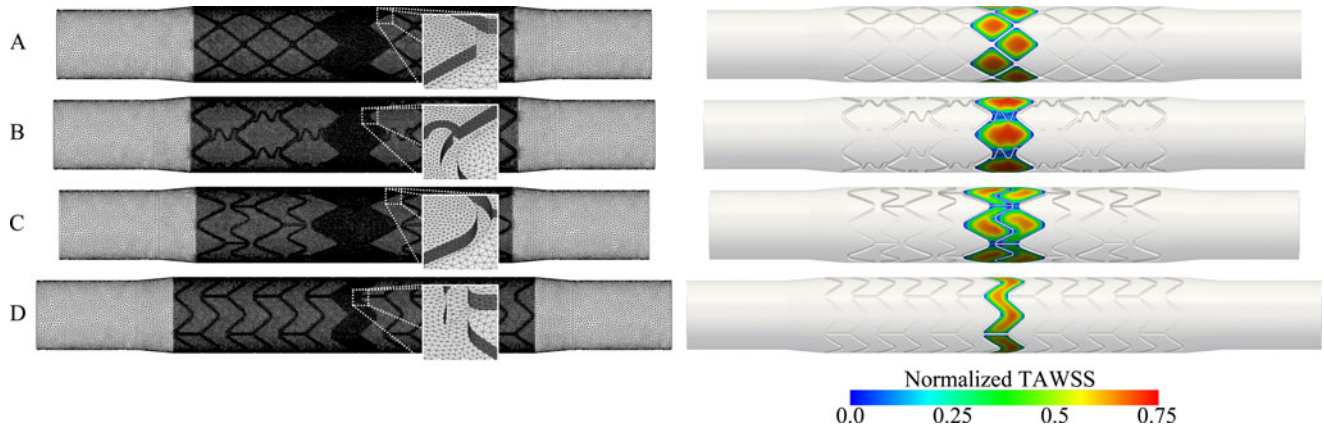

Fig. 3. (Left) Anisotropic meshes used for CFD. (Right) TAWSS depicted on the stent cells that are extracted and quantified during the optimization routine. TAWSS is shown normalized to the analytically computed value of TAWSS in an unstented portion of the vessel.

developed Womersly profile [26]. For the purposes of this investigation, the flow waveform was not scaled for vessels of varying diameters, since TAWSS is later normalized when analyzing the cost of the stent design. A three-element Windkessel approximation consisting of characteristic and distal resistances, as well as a capacitance term (i.e., R_c, R_d, and C), was applied at the outlet to replicate the physiologic impedance of the downstream vasculature as previously described [27]–[29]. Additionally, the vessel and stent were modeled as rigid and blood was assumed to be a Newtonian fluid with a density of 1.06 g/cm^3 and a viscosity of 4 cP. A time step of 3.3×10^{-4} s was required for a Courant, Friedrichs, and Lewy condition <1 for the smallest diameter vessel during peak flow and was therefore used for each CFD simulation. Periodicity was ensured by running simulations until the difference in the outlet pressure and flow between equivalent points in successive cardiac cycles was <1 mmHg and <1 mm^3/s.

C. Design Optimization Algorithm

The general form of the optimization problem in this investigation was to minimize $J(\mathbf{x})$ subject to $\mathbf{x}$ of the set $B = \{\mathbf{x}|a < \mathbf{x} < b\}$, where J is the cost function and $\mathbf{x}$ is the vessel diameter bounded by a and b. The formulation of the optimization cost function was based on the physiologic theory of TAWSS homeostasis, which suggests vessels remodel to maintain a nominal level of TAWSS [30], [31]. Favorable stented models were defined as those which would theoretically attenuate vascular remodeling within the stented region by minimizing the disparity between TAWSS in the stented region of the model ($\overline{\text{TAWSS}}_{\text{IS}}$) and the nominal level of TAWSS in the unstented segment of the model ($\overline{\text{TAWSS}}_{\text{US}}$). Thus, the cost of a stent model is expressed using a ratio of $\overline{\text{TAWSS}}_{\text{IS}}$ to $\overline{\text{TAWSS}}_{\text{US}}$ as

$$J = 1 - \frac{\overline{\text{TAWSS}}_{\text{IS}}}{\overline{\text{TAWSS}}_{\text{US}}} \tag{1}$$

in which $\overline{\text{TAWSS}}_{\text{IS}}$ is defined as the integration of TAWSS over the intrastrut surfaces s normalized to the area of those surfaces

$$\overline{\text{TAWSS}}_{\text{IS}} = \frac{\int_s \text{TAWSS} ds}{\int_s ds}. \tag{2}$$

The value of $\overline{\text{TAWSS}}_{\text{IS}}$ was computed over the intrastrut regions with the highest mesh resolution (see Fig. 3). For a given diameter, $\overline{\text{TAWSS}}_{\text{US}}$ was computed as

$$\overline{\text{TAWSS}}_{\text{US}} = \frac{4\mu Q}{\pi r^3} \tag{3}$$

where Q is the mean flow, μ is the viscosity, and r is the vessel radius.

A surrogate management framework (SMF) was implemented to determine the optimal vessel diameter for a given stent configuration [32]. The SMF optimization algorithm is a derivative-free pattern search method with an extensive mathematical convergence theory. The design space is defined as a discrete parameter mesh which may be refined to increase the accuracy of the optimal solution. The optimization method incorporates a surrogate model for efficient exploration of the design space in a search step, and guarantees convergence to a local minimum through a poll step that evaluates neighboring points using the mesh adaptive direct search (MADS) method [33]–[35]. The algorithm, illustrated in Fig. 4, consists of performing surrogate search steps until the search step fails, and poll steps to determine if a mesh local optimizer has been reached. The surrogate function provides an approximation of the true cost function which reduces the number of expensive function evaluations without sacrificing the convergence theory of the method, which depends solely on the poll step. The entire optimization framework was fully automated such that no user intervention was required. We refer the reader to [23] and [32] for more details about the computational framework and convergence theory of the optimization routine.

To determine the optimal vessel diameter for a given stent configuration, an initial parameter mesh was constructed for a range of vessel diameters between 2.0 and 5.0 mm with a

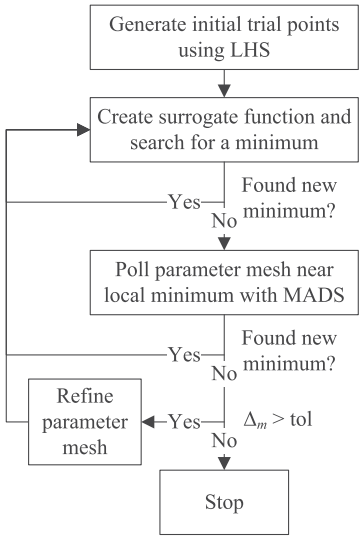

Fig. 4. Flowchart of the SMF optimization routine. The routine is initialized using LHS, and then uses search and MADS polling operations to converge on the optimal design parameter. The routine stops once a local minimum has been found and the resolution of the discrete parameter mesh Δ_m has been refined beyond a user defined tolerance (tol).

spacing of 0.5 mm. Latin hypercube sampling (LHS) was used to generate a well-distributed set of possible vessel diameters within the parameter space, which were evaluated to construct the initial surrogate function of the SMF algorithm. The parameter mesh was reduced three times by a factor of 4 during the course of the optimization, resulting in a final parameter mesh resolution of 0.03125 mm.

III. Results

The optimal vessel diameter was identified for four stent designs in various configurations (i.e., different values of N_C) for a total of 21 optimizations. The results of each optimization are summarized in Table II. Some optimizations converged to the boundary of the allowable vessel diameter range (see Table II). Only 6–7 function evaluations were necessary in these cases, corresponding to the three vessel diameters of the initial set of design points and the three-mesh refinements necessary to provide convergence to the boundary. In cases where the optimization did not converge to a boundary of the allowable vessel diameter range, the optimization routine required 9–18 function evaluations regardless of stent design. Each optimization required four to seven days to complete, depending on the number of function evaluations required.

The hemodynamically optimal vessel diameter increased as N_C increased for all stent designs (e.g., A—$N_C = 6$, $\phi =$ 2.63 mm versus $N_C = 7$, $\phi = 3.13$ mm). For designs A, B, and C, the cost function value of the optimal design also increased with increasing vessel diameter (e.g., A—$N_C = 6$, $J =$ 0.526 versus $N_C = 7$, $J = 0.535$). This trend is less apparent for design D, in which the optimal cost did not increase between the 4-2:2 and 5-2:3 designs or 6-2:2:2 and 7-2:2:3 designs.

TABLE II
Optimal cost and model parameters for each stent configuration

N_C	Cost	Vessel Diameter (mm)	Intrastrut Angle (°)	Number of Function Evaluations
Stent A				
5*	0.511	2.00	44.59	7
6	0.526	2.63	50.74	11
7	0.535	3.13	52.22	12
8	0.542	3.75	55.97	10
9	0.548	4.22	55.97	18
10	0.552	4.81	58.09	15
Stent B				
4*	0.538	2.00	61.42	6
5	0.560	2.66	68.12	15
6	0.572	3.50	79.96	9
7	0.581	4.00	77.17	9
8	0.587	4.75	82.45	9
Stent C				
4	0.582	2.09	47.13	10
6	0.611	3.88	66.69	12
8*	0.625	5	63.22	7
Stent D				
4 – 2:2	0.529	2.38	87.09	10
5 – 2:3	0.529	3.13	96.88	11
6 – 2:2:2	0.536	4.06	111.09	15
6 – 3:3	0.53	3.88	104.00	11
7 – 2:2:3	0.536	4.63	107.04	11
8 – 2:3:3*	0.537	5.00	97.25	7
9 – 3:3:3*	0.544	5.00	79.68	7

*Optimization converged to the boundary of the parameter space.

The intrastrut area as a function of d (i.e., cell expansion curve) for a single stent cell is plotted in Fig. 5. For the peak–peak stent designs (A and B), the cell expansion curve is a concave function. The cell expansion curve was a concave function for designs A and B. This relationship was linear for design D and nearly linear with a small degree of concavity for design C. The degree of expansion for each of the optimal models is also denoted in Fig. 5. The optimal intrastrut angle for the configurations of designs A, B, and C (A: 50°–58°, B: 68°–82°, C: 47°–67°) was generally smaller than that of design D (87°–107°).

Plots of the cost function relative to the vessel diameter are shown in Fig. 6. These plots can be used to identify the optimal stent configuration for any given vessel diameter. The optimal configuration is simply the curve with the minimum cost for a given vessel diameter. Similarly, an optimal vessel diameter range for each stent configuration can be estimated from the intersection of the cost function with adjacent stent configuration. For example, the cost curves for the $N_C = 5$ and $N_C = 6$ configurations of design A intersect at about 2.6 mm and the curves for the $N_C = 6$ and $N_C = 7$ configuration of design A intersect at about 3.2 mm. Thus, the optimal vessel diameter range for the $N_C = 6$ configuration of design A is between 2.6 and 3.2 mm. The optimal vessel diameter ranges for each stent design is denoted by the alternating white and gray boxes in Fig. 6. The 6-2:2:2, not the 6-3:3, stent configuration was used when computing the optimal vessel diameter range for design D, as

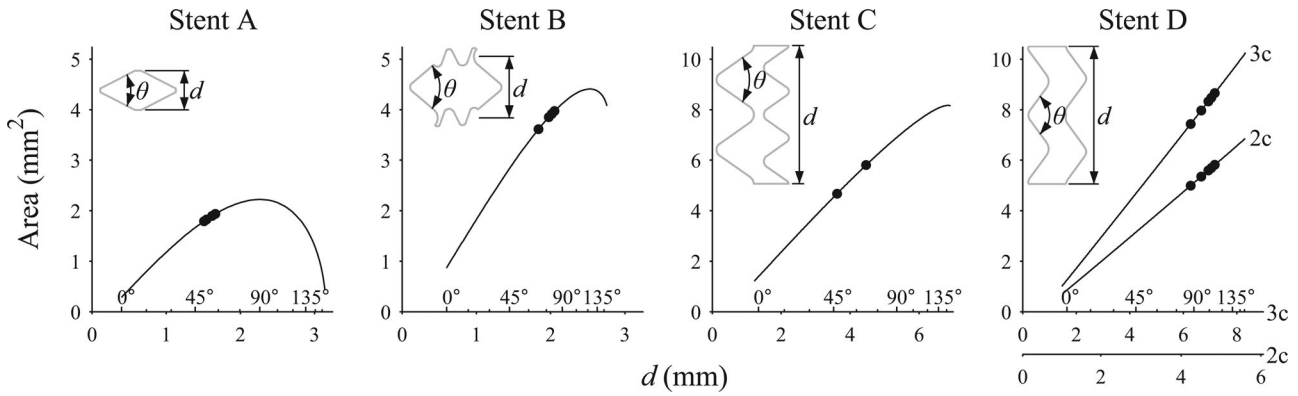

Fig. 5. Intrastrut area relative to the parameter d ("expansion curve") for a single cell of each stent design. For stent D, the expansion curves of both the two crown (2c) and three crown (3c) cells are shown. The value of d corresponding to the cell geometry of each optimal model is denoted along the curve as a black dot. Only configurations in which the optimization did not converge to a boundary are plotted. As an additional reference, the intrastrut angle (°) is also denoted above the x-axis.

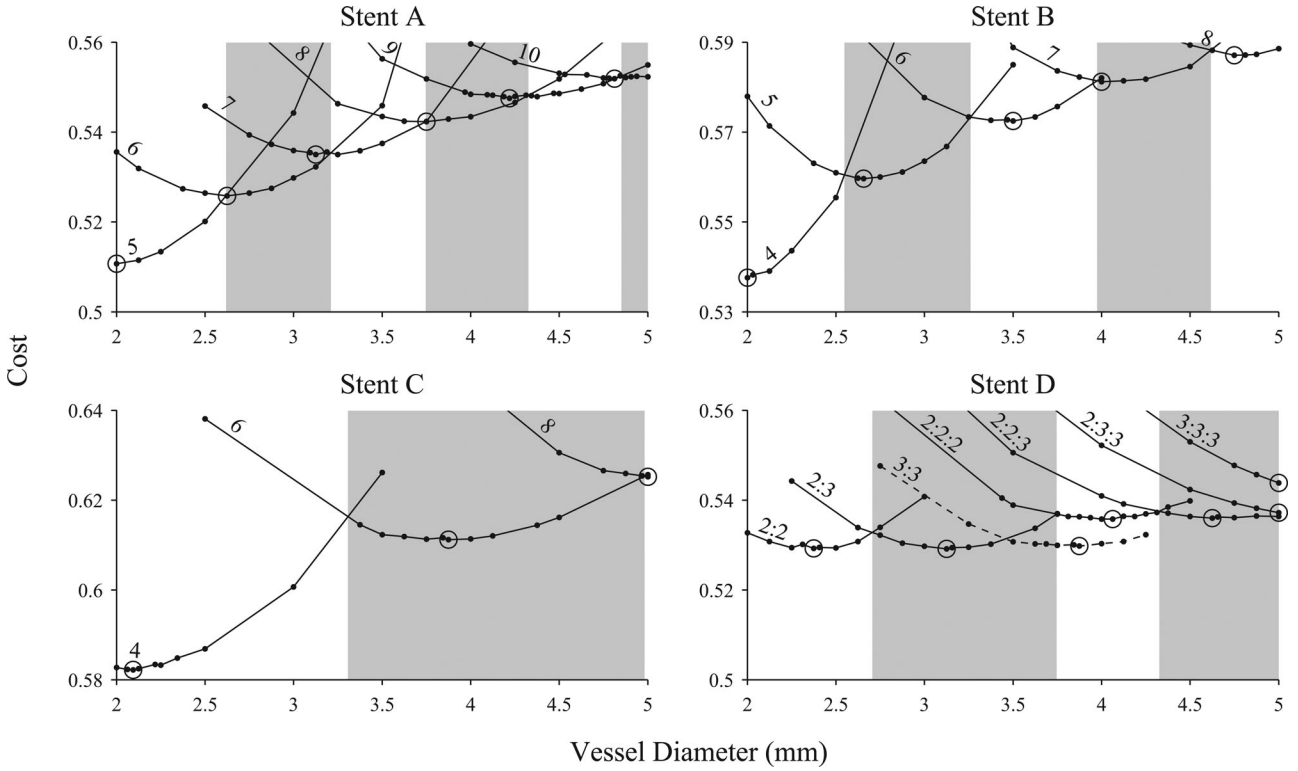

Fig. 6. Cost function versus the vessel diameter for the various configurations of each stent design. The stent configuration, or number of circumferential crowns, is denoted above each curve. The model corresponding to the optimal vessel diameter is circled for each stent configuration. The optimal vessel diameter range for each configuration is denoted by the alternating gray and white shaded areas. Both the 3:3 and 2:2:2 configurations of stent D represent a six crown stent, but the optimal vessel diameter range was not computed for the 3:3 configuration so it is denoted with a dotted line.

this is representative of the six crown version of the commercially available Multi-Link Vision stent.

Using a similar analysis, a comparison of the hemodynamic performance among the various stent designs is shown in Fig. 7 by plotting a least-cost curve for each design. The least-cost curve is constructed by extracting the minimum possible cost from among all the configurations of a stent design for entire vessel diameter range as plotted Fig. 6. A comparison of the least-cost curves indicates that in the most hemodynamically favorable configuration, stent design C performs worse than all other designs regardless of vessel diameter. Stent D is the best performing commercially inspired stent design, while the generic slotted-tube stent is the best-performing design in vessels less than 3.0 mm in diameter.

Given that the designs of stents B, C, and D closely resemble the commercially available BX Velocity, Express[2], and Multi-Link stents, respectively, a comparison of hemodynamically optimal vessel diameter range (see Fig. 6) to that of the

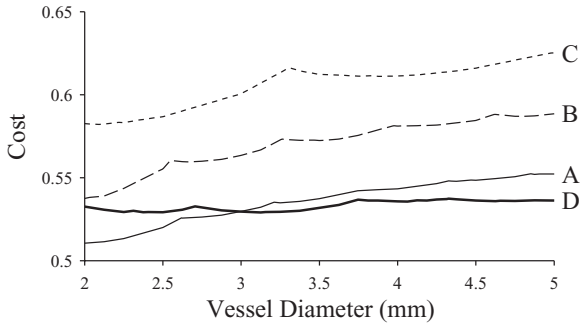

Fig. 7. Comparison of the least-cost curves of each stent design. The least-cost curve represents the best hemodynamic cost function value from all configurations of a given stent design for vessel diameters between 2.0 and 5.0 mm in diameter.

TABLE III
COMPARISON OF THE VESSEL DIAMETER RANGE RECOMMENDED BY STENT MANUFACTURERS (MFG. SUGGESTED) AND THE HEMODYNAMICALLY OPTIMAL VESSEL DIAMETER RANGE PREDICTED BY THE CFD SIMULATIONS

	Diameter Range (mm)		Intrastrut Angle Range (°)	
N_C	Mfg. Suggested	Simulated Optimal	Mfg. Suggested*	Simulated Optimal
(N/A)/A				
5		-2.58		-65.4
6		2.58-3.22		50.6-67.4
7		3.22-3.75		54.3-67.4
8		3.75-4.34		55.9-68.4
9		4.34-4.82		58.0-68.1
10		4.83-		58.7-
BX Velocity/B				
4		-2.55		-93.4
5		2.55-3.28		63.5-97.4
6	2.25-3.00	3.28-3.98	36.6-61.4	70.8-100.4
7	3.00-3.50	3.98-4.59	46.9-61.4	76.3-99.5
8		4.59-		78.5-
Express^2/C				
4		-3.24		-85.6
6	2.25-3.50	3.24-4.98	20.4-48.2	43.7-86.3
8	4.00-5.00	4.98-	36.8-54.1	53.7-
Multi-Link/D				
4 – 2:2		-2.71		-103.7
5 – 2:3		2.71-3.75		71.5-130.6
6 – 2:2:2	2.00-3.00	3.75-4.33	29.6-61.7	89.8-117.7
7 – 2:2:3		4.33-		89.1-
8 – 2:3:3				
9 – 3:3:3†	3.50-5.00		41.4-75.4	

* Manufacturer's suggested intrastrut angle was computed using the designs of stents B, C and D.
† Manufacturer's diameter range was based on a combination of the Multi-Link Vision and Ultra designs.

manufacturer's recommended diameter range is presented in Table III. The expanded geometry of a single stent crown at the minimum and maximum of each range is also depicted in Fig. 8. For any given vessel diameter, the commercial stents are configured with a greater number of crowns than the hemodynamically optimal configurations.

IV. DISCUSSION

Rates of restenosis are known to vary with stent design and geometry [14], [36]–[39]. Although vessel diameter is also an independent predictor of restenosis [1]–[4], the hemodynamic impact of altering the stent configuration based on vessel diameter has not previously been studied. In this investigation, we used an optimization routine coupled with CFD to identify the hemodynamically optimal vessel diameter for various configurations of a generic slotted tube and three commercially available stent designs. The results indicate that current commercial stent configurations have a greater number of circumferentially repeating stent crowns than in the hemodynamically optimal ones. Presumably, a larger number of stent crowns provide a greater amount of vessel scaffolding, but the current results demonstrate that this also increases the area of the vessel exposed to potentially deleterious levels of low TAWSS.

The unique framing of the optimization problem facilitated a thorough and detailed analysis of the relationship between vessel diameter and stent configuration without necessitating numerous optimizations. The main objective of the investigation was to identify the optimal value of N_C for a given stent design and vessel diameter. This naturally implies formulating the optimization problem to directly solve for the optimal value of N_C, while maintaining a constant vessel diameter. Instead this investigation used the reverse formulation to identify the optimal vessel diameter for a given N_C. This approach did not directly solve for N_C, but rather indirectly computed the optimal value of N_C for a given stent design and vessel diameter by examining the relationships between the cost function and vessel diameter (see Fig. 6). Moreover, the reverse formulation also enabled the analysis of the optimal intrastrut angle and quick computation of the optimal vessel diameter range for each stent configuration. The direct approach would require numerous optimizations to compute these parameters with the same resolution achieved using the reverse formulation.

The results of this investigation confirm and extend the findings of our previous CFD optimization of a generic slotted-tube stent, similar to stent A [23]. In our previous study, we determined the optimal value of N_C was dependent on the intrastrut angle, and the optimal intrastrut angle was computed to be about 40° for the two vessel sizes analyzed. As shown by the intrastrut angles of the optimal models (see Table II), the small range of optimal angles for each stent design supports our previous conclusion that the optimal value of N_C is dependent on the intrastrut angle. However, contrary to the findings of our previous study, the current results indicate that the optimal intrastrut angle is somewhat dependent on vessel size. The optimization routine generally converged to designs with a smaller intrastrut angle in small diameter vessels (see Table II). The discrepancy between the findings of these studies is likely caused by the difference in design constraints used in each study. In our previous study, the intrastrut area was constrained to 1, 2, or 3 mm^2, and optimization were only performed with 2.25- and 3.0-mm diameter vessels [23]. The current results were obtained by constraining the stent strut dimensions and allowing the vessel diameter, and subsequently the intrastrut area, to vary. The current constraints mimic the realistic deployment of a stent and result in a better approximation of the optimal intrastrut angle. Thus, the optimal intrastrut angle for a slotted-tube design is more likely

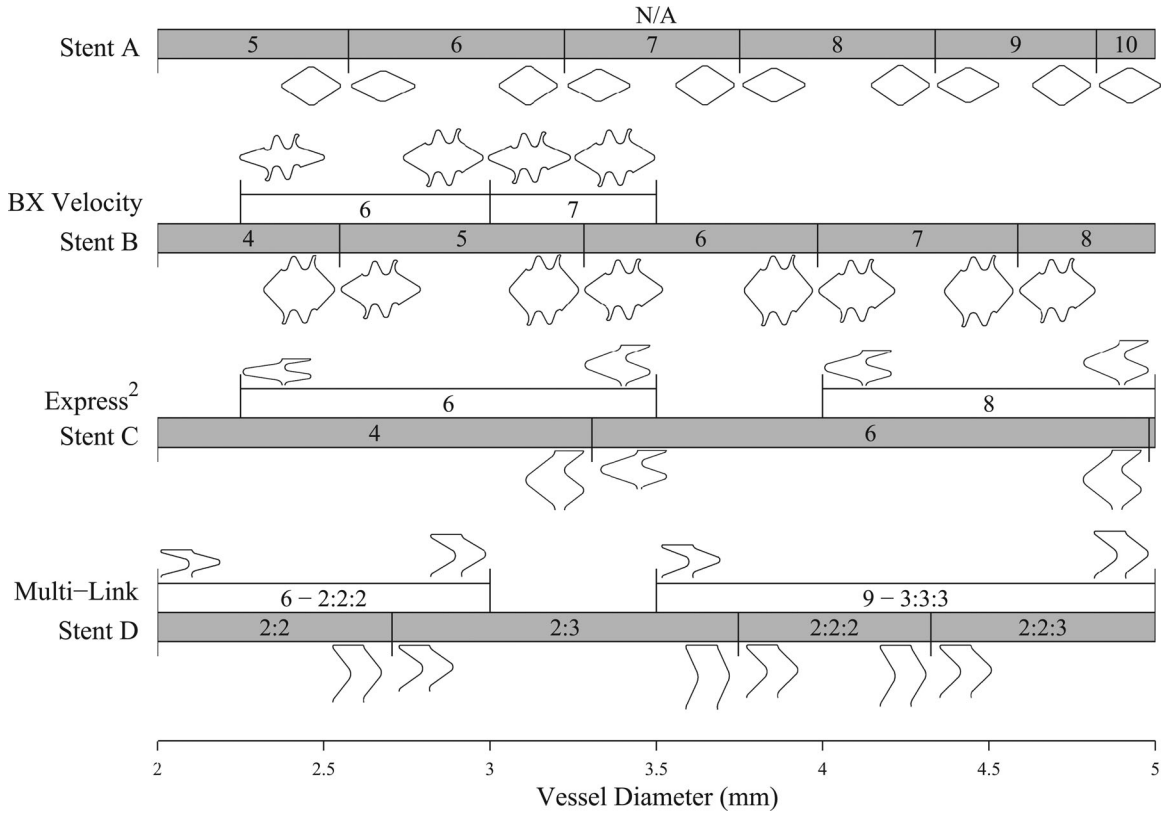

Fig. 8. Comparison of the vessel diameter range of commercially available stents with the hemodynamically optimal diameter range. The expanded geometry of a single circumferential crown corresponding to the minimum and maximum cell expansion of each range is also shown.

between 50° and 60°, as opposed to the previously reported value of 40°.

The current results indicate the optimal intrastrut angle for stent designs A (50°–58°), B (68°–82°), and C (47°–67°) were less than that of the design D (87°–107°). This finding is likely explained by the differences in the connection types of each stent design, which produce different relationships between the circumferential distance between adjacent struts and intrastrut area (see Fig. 5). This relationship is linear for stents with peak–valley connections (stent D), so the intrastrut area is directly proportional to the vessel diameter. For peak–peak connections (stents A and B), this relationship is nearly linear for small values of d (i.e., small diameter vessels), but is increasingly concave for larger values of d (i.e., large diameter vessels). Thus, as a peak–peak type stent expands to a large diameter, decreases in TAWSS resulting from strut misalignment are not counteracted by as large an increase in TAWSS resulting from a greater intrastrut area. It is, therefore, not surprising that the optimal intrastrut angle was less for peak–peak designs, which further confirms our original hypothesis that the hemodynamically optimal vessel diameter for a given stent configuration represents a balance between the competing effects of strut misalignment and increasing intrastrut area.

The cost of the models corresponding to the optimal vessel diameter of a given stent configuration increased with increasing vessel diameter and N_C for designs A, B, and C. This relationship causes the value of the optimal vessel diameter to be skewed toward the low end, or fall completely outside, of the optimal vessel diameter range for most configurations (see Fig. 6). For example, the optimal vessel diameter for the seven crown configuration of design B is 4 mm, while the optimal vessel diameter range of this configuration is about 4–4.60 mm. The lack of this trend in stent D likely arises from the combined use of two and three crest cell geometries. Incorporating a three-cell geometry into the stent configuration generally resulted in lower costs than the two crest cell design as evident by comparison of the 6-2:2:2 and 6-3:3 optimization (see Fig. 6). Although the two stent designs have the same number of crowns, the 6-3:3 stent has fewer axial connections and a lower associated cost (0.536 versus 0.530). This result is consistent with the findings of He *et al.* which demonstrated that the presence of axial connectors for peak–peak stent designs decreases TAWSS [18].

The least-cost curves (see Fig. 7) suggest that the relative ranking of performance (best to worst) of the commercially inspired stent designs considered is D (Multi-Link), B (BX Velocity), and C (Express^2). It should be noted that some commercial versions of stent D include a flexible connector link that would likely produce a greater area of low TAWSS than was computed here which may affect this ranking. While these ranking provide insight into relative performance of commercial stents, they cannot be used to draw any general conclusions about the performance of peak–peak, peak–valley or hybrid designs as the prescribed strut thickness and width varied between the designs to mimic the dimensions of the commercially available stents. This investigation does highlight the superior adaptability of the peak–peak and peak–valley designs to various vessel diameters

as compared to the hybrid design (see Fig. 8). The number of circumferential crowns of the hybrid design can only be incremented by a factor of two due to the cell geometry, whereas the other designs allow for unit increments.

Compared to configurations of commercially available stents, the current results suggest that hemodynamically optimal stents contain fewer circumferentially repeating crowns, which result in greater spacing between struts. While an increase in strut spacing is hemodynamically advantageous, this may adversely affect other stent design criteria. Specifically, increasing strut spacing may reduce the radial strength and subsequently the radial displacement of the stent [40], [41]. For DES stents, increased strut spacing reduces the uniformity of drug release along with the intrastrut drug concentration [42]. Interestingly, a previous study by Iakovou *et al.* demonstrated that increased strut spacing was not associated with unfavorable clinical outcomes for the Cypher stent, the DES version of the BX Velocity [43]. In this study, six crown Cypher stents were overdilated beyond the suggested 3.0-mm diameter maximum for 3.5–4.0 diameter vessels, similar to the hemodynamically optimal vessel range for this stent configuration. Overdilation was not associated with increased late lumen loss or binary restenosis rate. However, this study was only performed in large diameter vessels which are generally associated with a decreased rate of restenosis and is unclear if these results would translate to smaller vessels. Similarly, overexpansion of the Express^2 and Multi-Link designs has not been studied in detail.

The current results should be interpreted within the constraints of several potential limitations. Most notably, each vessel was modeled as an ideal cylinder and may not represent the actual vessel geometry following stent deployment. A finite-element simulation of the stent expansion may be the best method for determining the expanded geometry of the stent and vessel. However, this approach would further increase the computational cost of the already computationally expensive optimization routine and would require the nontrivial process of converting a discrete finite-element mesh into a highly anisotropic CFD meshes on specific model surfaces [44], as was the case in this investigation. Since a finite-element approach was not pursued in this investigation, the results of this investigation do not account for malapposition of stent struts and vessel prolapse which have been shown to affect the distribution of TAWSS [45]–[47]. Future studies should consider adopting this approach similar to De Santis *et al.* to better replicate the physiologic geometry of a stented artery [45]. Also, the vessel models in this investigation employ a rigid wall assumption for all CFD simulations. Since the compliance of stented arteries has been shown to be nearly zero, a rigid wall assumption is likely valid within the stented region that is quantified during the optimization routine [26].

The choice of cost function may influence the results of the optimization algorithm. This investigation used a cost function based on TAWSS within the stented region since areas of low TAWSS are known to correlate with neointimal growth and endothelialization of stent struts [7]–[9]. Other clinically relevant hemodynamic indices, such as WSS gradient and oscillatory shear index, could also be used as additional cost functions [15]. Additional research is necessary to understand how these indices might affect the identification of optimal stent designs.

This study attempted to include some of the most widely used stent geometries at this time. The companies referred to here may now have, or be developing, newer stents for which the demonstrated optimization techniques could be used to identify the hemodynamically optimal design configurations. The current results describe some general hemodynamic characteristics of peak–peak, peak–valley stent and hybrid designs which are likely applicable to new designs without a complete optimization analysis. However, the variability among designs within these categories, as shown by the difference in optimal configurations of stents A and B (see Table II and Fig. 8), suggests a complete optimization analysis is necessary for each unique stent design.

The optimization methodology presented here was developed to understand the relationship between stent configuration and vessel diameter, and possibly improve stent design for treating small vessel lesions. With a few modifications to the vessel-generation and cost-quantification procedures, this methodology could be used to investigate potential design improvements of commercial stents for treating other difficult lesions subsets such as those in the left main coronary artery where efficacy data for most stents are limited and local disruptions in the vicinity of the bifurcation increase the potential for flow patterns linked to neointimal growth and thrombus formation [48].

V. Conclusion

In summary, the current investigation used 3-D CFD coupled with an efficient derivative-free optimization routine to identify the optimal vessel diameter for various configurations of a generic slotted-tube and commercially available stents. The results indicate that the optimal vessel diameter for a given stent configuration produces a stent-cell geometry in which the competing hemodynamic effects of strut misalignment and increasing intrastrut areas are balanced. For each commercial stent design, it was generally found that current stent designs incorporate a greater number of circumferentially repeating stent crowns than hemodynamically optimal stent designs, which may subject the vessel to potential deleterious levels of low TAWSS. This may partially explain why rates of restenosis remain high after stent implantation in small diameter vessels.

Acknowledgment

The authors recognize Dr. N. Wilson of Open Source Medical Software Corporation for technical assistance.

References

[1] S. Elezi, A. Kastrati, F. J. Neumann, M. Hadamitzky, J. Dirschinger, and A. Schömig, "Vessel size and long-term outcome after coronary stent placement," *Circulation*, vol. 98, no. 18, pp. 1875–1880, 1998.

[2] I. C. Hsieh, C. C. Chien, H. J. Chang, M. S. Chern, K. C. Hung, F. C. Lin, and D. Wu, "Acute and long-term outcomes of stenting in coronary vessel $>$3.0 mm, 3.0–2.5 mm, and $<$2.5 mm," *Catheter Cardiovasc. Interv.*, vol. 53, no. 3, pp. 314–322, 2001.

[3] A. Kastrati, A. Dibra, J. Mehilli, S. Mayer, S. Pinieck, J. Pache, J. Dirschinger, and A. Schömig, "Predictive factors of restenosis after coronary implantation of sirolimus- or paclitaxel-eluting stents," *Circulation*, vol. 113, no. 19, pp. 2293–300, 2006.

[4] B. Cortese, A. Bertoletti, S. De Matteis, G. B. Danzi, and A. Kastrati, "Drug-eluting stents perform better than bare metal stents in small coronary vessels: A meta-analysis of randomised and observational clinical studies with mid-term follow up," *Int. J. Cardiol.*, 2011. [Online]. DOI: http://dx.doi.org/10.1016/j.ijcard.2011.04.016, 2012.

[5] M. C. Morice, "Stenting for small coronary vessels," *J. Invasive Cardiol.*, vol. 15, no. 7, pp. 377–379, 2003.

[6] D. H. Steinberg, S. Mishra, A. Javaid, T. L. P. Slottow, A. N. Buch, P. Roy, T. Okabe, K. a. Smith, R. Torguson, Z. Xue, A. D. Pichard, L. F. Satler, K. M. Kent, W. O. Suddath, and R. Waksman, "Comparison of effectiveness of bare metal stents versus drug-eluting stents in large ($\geq$3.5 mm) coronary arteries," *Amer. J. Cardiol.*, vol. 99, no. 5, pp. 599–602, 2007.

[7] S. G. Carlier, L. C. a. van Damme, C. P. Blommerde, J. J. Wentzel, G. van Langehove, S. Verheye, M. M. Kockx, M. W. M. Knaapen, C. Cheng, F. Gijsen, D. J. Duncker, N. Stergiopulos, C. J. Slager, P. W. Serruys, and R. Krams, "Augmentation of wall shear stress inhibits neointimal hyperplasia after stent implantation: inhibition through reduction of inflammation?" *Circulation*, vol. 107, no. 21, pp. 2741–2746, 2003.

[8] J. F. LaDisa, L. E. Olson, R. C. Molthen, D. A. Hettrick, P. F. Pratt, M. D. Hardel, J. R. Kersten, D. C. Warltier, and P. S. Pagel, "Alterations in wall shear stress predict sites of neointimal hyperplasia after stent implantation in rabbit iliac arteries," *Amer. J. Physiol. Heart Circ. Physiol.*, vol. 288, no. 5, pp. H2465–H2475, 2005.

[9] J. J. Wentzel, R. Krams, J. C. Schuurbiers, J. A. Oomen, J. Kloet, W. J. van Der Giessen, P. W. Serruys, and C. J. Slager, "Relationship between neointimal thickness and shear stress after Wallstent implantation in human coronary arteries," *Circulation*, vol. 103, no. 13, pp. 1740–1745, 2001.

[10] E. A. Sprague, J. Luo, and J. C. Palmaz, "Endothelial cell migration onto metal stent surfaces under static and flow conditions," *J. Long Term Eff. Med. Implants*, vol. 10, no. 1–2, pp. 97–110, 2000.

[11] A. V. Finn, G. Nakazawa, M. Joner, F. D. Kolodgie, E. K. Mont, H. K. Gold, and R. Virmani, "Vascular responses to drug eluting stents: importance of delayed healing," *Arterioscler Thromb. Vasc. Biol.*, vol. 27, no. 7, pp. 1500–1510, 2007.

[12] M. Joner, G. Nakazawa, A. V. Finn, S. C. Quee, L. Coleman, E. Acampado, P. S. Wilson, K. Skorija, Q. Cheng, X. Xu, H. K. Gold, F. D. Kolodgie, and R. Virmani, "Endothelial cell recovery between comparator polymer-based drug-eluting stents," *J. Amer. Coll. Cardiol.*, vol. 52, no. 5, pp. 333–342, 2008.

[13] J. Kotani, M. Awata, S. Nanto, M. Uematsu, F. Oshima, H. Minamiguchi, G. S. Mintz, and S. Nagata, "Incomplete neointimal coverage of sirolimus-eluting stents: angioscopic findings," *J. Amer. Coll. Cardiol.*, vol. 47, no. 10, pp. 2108–2111, 2006.

[14] J. F. LaDisa, L. E. Olson, I. Guler, D. A. Hettrick, S. H. Audi, J. R. Kersten, D. C. Warltier, and P. S. Pagel, "Stent design properties and deployment ratio influence indexes of wall shear stress: A three-dimensional computational fluid dynamics investigation within a normal artery," *J. Appl. Physiol.*, vol. 97, no. 1, pp. 424–430, 2004.

[15] J. B. Murphy and F. J. Boyle, "A full-range, multivariable, CFD-based methodology to identify abnormal near-wall hemodynamics in a stented coronary artery," *Biorheology*, vol. 47, no. 2, pp. 117–132, 2010.

[16] D. Rajamohan, R. K. Banerjee, L. H. Back, A. a. Ibrahim, and M. A. Jog, "Developing pulsatile flow in a deployed coronary stent," *J. Biomech. Eng.*, vol. 128, no. 3, pp. 347–359, 2006.

[17] J. F. LaDisa, L. E. Olson, D. A. Hettrick, D. C. Warltier, J. R. Kersten, and P. S. Pagel, "Axial stent strut angle influences wall shear stress after stent implantation: Analysis using 3D computational fluid dynamics models of stent foreshortening," *Biomed. Eng. Online*, vol. 59, no. 59, 2005, DOI: http://dx.doi.org/10.1186/1475-925X-4-59.

[18] Y. He, N. Duraiswamy, A. O. Frank, and J. E. Moore, "Blood flow in stented arteries: A parametric comparison of strut design patterns in three dimensions.," *J. Biomech. Eng.*, vol. 127, no. 4, pp. 637–647, 2005.

[19] A. Blouza, L. Dumas, and I. M'Baye, "Multiobjective optimization of a stent in a fluid-structure context," in *Proc. 2008 GECCO Conf. Companion Genetic Evolutionary Comput.*, 2008, pp. 2055–2060.

[20] K. Srinivas, T. Nakayama, M. Ohta, S. Obayashi, and T. Yamaguchi, "Studies on design optimization of coronary stents," *J. Med. Devices*, vol. 2, no. 1, p. 011004, 2008, DOI: http://dx.doi.org/10.1115/1.2885145.

[21] M. A. Atherton and R. A. Bates, "Robust optimization of cardiovascular stents: A comparison of methods," *Eng. Optimiz*, vol. 36, no. 2, pp. 207–217, 2004.

[22] S. Pant, G. Limbert, N. P. Curzen, and N. W. Bressloff, "Multiobjective design optimisation of coronary stents," *Biomaterials*, vol. 32, no. 31, pp. 7755–7773, 2011.

[23] T. J. Gundert, A. L. Marsden, W. Yang, and J. F. LaDisa, Jr, "Optimization of cardiovascular stent design using computational fluid dynamics," *J. Biomech. Eng.*, vol. 134, no. 1, p. 011002, 2012, DOI: http://dx.doi.org/10.1115/1.4005542.

[24] D. Stoeckel, C. Bonsignore, S. Duda, and M. Dunitz, "A survey of stent designs," *Minimum Invasive Therapy*, vol. 11, no. 4, pp. 137–147, 2002.

[25] J. M. Garasic, E. R. Edelman, J. C. Squire, P. Seifert, M. S. Williams, and C. Rogers, "Stent and artery geometry determine intimal thickening independent of arterial injury," *Circulation*, vol. 101, no. 7, pp. 812–818, 2000.

[26] J. F. LaDisa, D. A. Hettrick, L. E. Olson, I. Guler, E. R. Gross, T. T. Kress, J. R. Kersten, D. C. Warltier, and P. S. Pagel, "Stent implantation alters coronary artery hemodynamics and wall shear stress during maximal vasodilation," *J. Appl. Physiol*, vol. 93, no. 6, pp. 1939–1946, 2002.

[27] I. E. Vignon-Clementel, C. A. Figueroa, K. E. Jansen, and C. a. Taylor, "Outflow boundary conditions for three-dimensional finite element modeling of blood flow and pressure in arteries," *Comput. Methods Appl. Mech. Eng.*, vol. 195, no. 29–32, pp. 3776–3796, 2006.

[28] A. R. Williams, B.-K. Koo, T. J. Gundert, P. J. Fitzgerald, and J. F. LaDisa, "Local hemodynamic changes caused by main branch stent implantation and subsequent virtual side branch balloon angioplasty in a representative coronary bifurcation," *J. Appl. Physiol*, vol. 109, no. 2, pp. 532–540, 2010.

[29] L. M. Ellwein, H. Otake, T. J. Gundert, B.-K. Koo, T. Shinke, Y. Honda, J. Shite, and J. F. LaDisa, "Optical coherence tomography for patient-specific 3D artery reconstruction and evaluation of wall shear stress in a left circumflex coronary artery," *Cardiovasc. Eng. Technol.*, vol. 2, no. 3, pp. 212–227, 2011.

[30] S. Glagov, E. Weisenberg, C. K. Zarins, R. Stankunavicius, and G. J. Kolettis, "Compensatory enlargement of human atherosclerotic coronary arteries," *N Engl. J. Med.*, vol. 316, no. 22, pp. 1371–1375, 1987.

[31] A. Kamiya and T. Togawa, "Adaptive regulation of wall shear stress to flow change in the canine carotid artery," *Amer. J. Physiol Heart Circ. Physiol*, vol. 239, no. 1, pp. H14–H21, 1980.

[32] A. L. Marsden, J. A. Feinstein, and C. A. Taylor, "A computational framework for derivative-free optimization of cardiovascular geometries," *Comput. Methods Appl. Mech. Eng.*, vol. 197, no. 21–24, pp. 1890–1905, 2008.

[33] C. Audet and J. E. Dennis, "Mesh adaptive direct search algorithms for constrained optimization," *SIAM J. Optimiz.*, vol. 17, no. 1, pp. 188–217, 2006.

[34] A. L. Marsden, M. Wang, J. E. Dennis Jr., and P. Moin, "Optimal aeroacoustic shape design using the surrogate management framework," *Optim. Eng.*, vol. 5, no. 2, pp. 235–262, 2004.

[35] A. L. Marsden, M. Wang, J. E. Dennis, and P. Moin, "Trailing-edge noise reduction using derivative-free optimization and large-eddy simulation," *J. Fluid Mech.*, vol. 572, pp. 13–36, 2007.

[36] D. R. McLean and N. L. Eiger, "Stent design: Implications for restenosis," *Rev. Cardiovasc. Med.*, vol. 3, suppl. 5, pp. S16–S22, 2002.

[37] C. Rogers and E. R. Edelman, "Endovascular stent design dictates experimental restenosis and thrombosis," *Circulation*, vol. 91, no. 12, pp. 2995–3001, 1995.

[38] J. Pache, A. Dibra, J. Mehilli, A. Schömig, and A. Kastrati, "Intracoronary stenting and angiographic results: strut thickness effect on restenosis outcome (ISAR-STEREO-2) trial," *J. Amer. Coll. Cardiol*, vol. 41, no. 8, pp. 1283–1288, 2003.

[39] J. Hausleiter, A. Kastrati, J. Mehilli, H. Schühlen, J. Pache, F. Dotzer, J. Dirschinger, and A. Schömig, "Predictive factors for early cardiac events and angiographic restenosis after coronary stent placement in small coronary arteries," *J. Amer. Coll. Cardiol*, vol. 40, no. 5, pp. 882–889, 2002.

[40] J. Bedoya, C. a. Meyer, L. H. Timmins, M. R. Moreno, and J. E. Moore, "Effects of stent design parameters on normal artery wall mechanics," *J. Biomech. Eng.*, vol. 128, no. 5, pp. 757–765, 2006.

[41] L. H. Timmins, M. R. Moreno, C. a. Meyer, J. C. Criscione, A. Rachev, and J. E. Moore, "Stented artery biomechanics and device design optimization," *Med. Biol. Eng. Comput.*, vol. 45, no. 5, pp. 505–513, 2007.

[42] B. Balakrishnan, A. R. Tzafriri, P. Seifert, A. Groothuis, C. Rogers, and E. R. Edelman, "Strut position, blood flow, and drug deposition: implications for single and overlapping drug-eluting stents," *Circulation*, vol. 111, no. 22, pp. 2958–2965, 2005.

[43] I. Iakovou, G. Stankovic, M. Montorfano, F. Airoldi, A. Chieffo, G. M. Sangiorgi, M. Carlino, N. Corvaja, M. Iassen, R. Rogacka, G. Vitrella, and A. Colombo, "Is overdilatation of 3.0 mm sirolimus-eluting stent associated with a higher restenosis rate?" *Catheter Cardiovasc. Interv.*, vol. 64, no. 2, pp. 129–133, 2005.

[44] R. Balossino, F. Gervaso, F. Migliavacca, and G. Dubini, "Effects of different stent designs on local hemodynamics in stented arteries," *J. Biomech.*, vol. 41, no. 5, pp. 1053–1061, 2008.

[45] G. De Santis, M. Conti, B. Trachet, T. De Schryver, M. De Beule, J. Degroote, J. Vierendeels, F. Auricchio, P. Segers, P. Verdonck, and B. Verhegghe, "Haemodynamic impact of stent-vessel (mal)apposition following carotid artery stenting: Mind the gaps!" *Comput. Methods Biomech. Biomed. Eng.*, (2011), [Online]. DOI: http://dx.doi.org/10.1080/10255842.2011.629997.

[46] J. F. LaDisa, L. E. Olson, I. Guler, D. A. Hettrick, J. R. Kersten, D. C. Warltier, and P. S. Pagel, "Circumferential vascular deformation after stent implantation alters wall shear stress evaluated with time-dependent 3D computational fluid dynamics models," *J. Appl. Physiol.*, vol. 98, no. 3, pp. 947–57, 2005.

[47] J. Murphy and F. Boyle, "Assessment of the effects of increasing levels of physiological realism in the computational fluid dynamics analyses of implanted coronary stents," in *Engineering in Medicine and Biology Society, 2008. in Proc. IEEE 30th Annual Int. Conf.*, 2008. pp. 5906–5909.

[48] M. Ragosta, S. Dee, I. J. Sarembock, L. C. Lipson, L. W. Gimple, and E. R. Powers, "Prevalence of unfavorable angiographic characteristics for percutaneous intervention in patients with unprotected left main coronary artery disease," *Catheter Cardiovasc. Interv.*, vol. 68, no. 3, pp. 357–62, 2006.

Authors' photographs and biographies not available at the time of publication.